

Interval Bound Propagation–aided Few-shot Learning

Shounak Datta, Sankha Subhra Mullick, Swagatam Das

Indian Statistical Institute

Abstract. Few-shot learning aims to transfer the knowledge acquired from training on a diverse set of tasks, from a given task distribution, to generalize to unseen tasks, from the same distribution, with a limited amount of labeled data. The underlying requirement for effective few-shot generalization is to learn a good representation of the task manifold. One way to encourage this is to preserve local neighborhoods in the feature space learned by the few-shot learner. To this end, we introduce the notion of interval bounds from the provably robust training literature to few-shot learning. The interval bounds are used to characterize neighborhoods around the training tasks. These neighborhoods can then be preserved by minimizing the distance between a task and its respective bounds. We further introduce a novel strategy to artificially form new tasks for training by interpolating between the available tasks and their respective interval bounds, to aid in cases with a scarcity of tasks. We apply our framework to both model-agnostic meta-learning as well as prototype-based metric-learning paradigms. The efficacy of our proposed approach is evident from the improved performance on several datasets from diverse domains in comparison to a sizable number of recent competitors.

Keywords: Few-shot learning, Interval bound propagation, Meta-learning, Metric-learning, Few-task training.

1 Introduction

Few-shot learning methods attempt to have better generalization capability such that they can leverage the knowledge acquired by training on a large pool of tasks from a given task distribution, and adapt to unseen tasks from the same distribution, using only a few labeled examples. Since the unseen tasks are sampled from the same underlying manifold governing the task distribution, learning a good representation of the task manifold is a natural way to effectively generalize to the new tasks using a limited amount of labeled data. Manifold learning methods [24,20,14] function by aiming to preserve the neighborhoods from the high-dimensional manifold during the lower dimensional projection. Similarly, the feature embedding learned by the few-shot learner should conserve the neighborhoods from the high-dimensional task manifold. However, existing few-shot learning methods lack an explicit mechanism for achieving this. Therefore, in

this work, we develop a method to explicitly constrain the feature embedding in an attempt to preserve neighborhoods from the high-dimensional task manifold.

The proposed approach incorporates the notion of interval bounds from the provably robust training literature [6] into the few-shot learning framework. Concretely, as shown in Figure 1, we use interval arithmetic to define a small ϵ -neighborhood around each few-shot training task. Interval Bound Propagation (IBP) [6] is then employed to obtain the bounding box around the mapping of the ϵ -neighborhood in the feature embedding space. In addition to optimizing the few-shot classification objective, we also attempt to preserve the ϵ -neighborhoods by minimizing the distance between a task and its respective bounds obtained from IBP. It is important to notice that this setup is distinct from provably robust training for few-shot learning in that we do not attempt to minimize (or calculate for that matter) the worst-case classification loss.

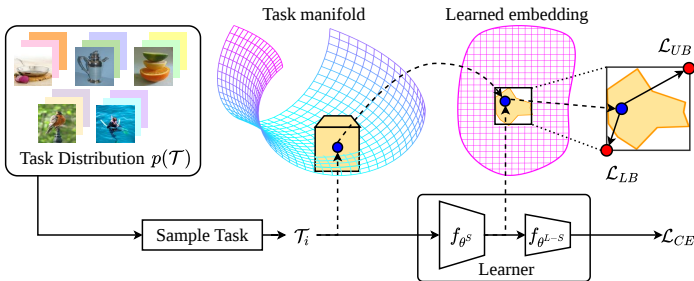


Fig. 1. Illustration of the proposed interval bound propagation-aided few-shot learning setup (best viewed in color): We use interval arithmetic to define a small ϵ -neighborhood around a training task \mathcal{T}_i sampled from the task distribution $p(\mathcal{T})$. IBP is then used to obtain the bounding box around the mapping of the said neighborhood in the embedding space f_{θ^S} given by the first S layers of the learner f_{θ} . While training the learner f_{θ} to minimize the classification loss \mathcal{L}_{CE} on the query set \mathcal{D}_i^q , we additionally attempt to minimize the losses \mathcal{L}_{LB} and \mathcal{L}_{UB} , forcing the ϵ -neighborhood to be compact in the embedding space as well.

Few-shot learning typically requires a large number of diverse training tasks. However, real-world few-shot learning scenarios like a medical application may not have sufficient training tasks, due to various constraints such as data collection costs, privacy concerns, and/or data availability in newer domains. In such scenarios, few-shot learning methods are prone to overfit on the training tasks, thus limiting the ability to generalization to unseen tasks. Various methods have been proposed to mitigate this problem using approaches such as explicit regularization of the learning model [8,29], intra-task augmentation [10,15,27], and inter-task interpolation to construct new artificial tasks [28]. While inter-task interpolation has been shown to be the most effective among these existing approaches, it suffers from the limitation that the artificially created tasks may be generated away from the task manifold depending on the curvature of the

feature embedding space, as there is no natural way to select pairs of task which are close to each other on the manifold (see Figure 2(a)). The interval bounds obtained using IBP, on the other hand, are likely to be close to the task embedding as we explicitly minimize the distance between a task and its interval bounds. Therefore, we also propose a mechanism to construct artificial tasks in task-scarce scenarios by interpolating between a task and its corresponding IBP bounds (see Figure 2(b)).

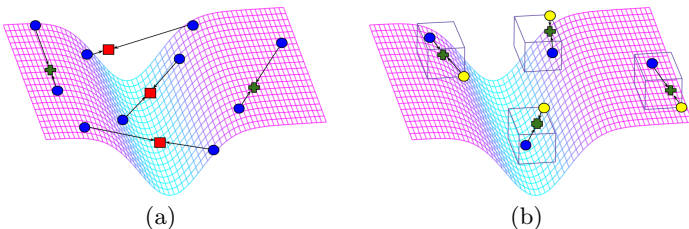


Fig. 2. Interval bound-based task interpolation (best viewed in color): (a) Existing inter-task interpolation methods create new artificial tasks by combining pairs of original tasks (blue ball). However, depending on how flat the task manifold embedding is at the layer where interpolation is performed, the artificial tasks may either be created close to the task-manifold (green cross), or away from the task manifold (red box). (b) The proposed interval bound-based task interpolation creates artificial tasks by combining an original task with one of its interval bounds (yellow ball). Such artificial tasks are likely to be in the vicinity of the task manifold as the interval bounds are forced to be close to the task embedding by the losses \mathcal{L}_{LB} and \mathcal{L}_{UB} .

In essence, the key contributions made in this article advances the existing literature in the following ways: **(1)** In Section 4.1-4.2, we synergize few-shot learning with interval bound propagation [6] to explicitly lend the ability to preserve task neighborhoods in the feature embedding space of the few-shot learner. **(2)** In Section 4.3, we further propose an interval bound-based task interpolation technique which is able to create new tasks (as opposed to augmenting each individual task [10,15,27]), by interpolating between a task sampled from the task distribution and its interval bounds. **(3)** Unlike existing inter-task interpolation methods [28] which require batches of paired tasks, the proposed methods act on individual tasks and hence are compatible with both meta-learning as well as metric-learning paradigms of few-shot learning.

In Section 5, we empirically demonstrate the effectiveness of our proposed approach on both gradient-based meta-learning and prototype-based metric-learning on five real-world datasets from various domains, outperforming 20 notable and recent prior methods. We also undertake ablation studies and cross domain transferability analysis for the two proposed methods. Finally, we make concluding remarks and also discuss limitation and future scopes of research in Section 6.

2 Related works

Manifold learning: IBP [6] was proposed for provably robust training of classifiers against adversarial attacks. We repurpose IBP to define ϵ -neighborhoods around few-shot learning tasks and constrain the learned feature embedding to preserve the said neighborhoods. This is similar in spirit to traditional manifold learning approaches such as ISOMAP [24], LLE [20], t-SNE [14], etc.

Task augmentation: In order to train on datasets with a limited number of tasks, some works directly impose regularization on the few-shot learner [8,29]. Another line of work performs data augmentation on the individual tasks [10,15,27]. Finally, a third direction is to employ inter-task interpolation to mitigate task scarcity [28]. Our approach is similar to the latter category in that we directly create new artificial tasks but also differs from all of the above-mentioned methods in that we neither undertake intra-task augmentation nor inter-task interpolation.

3 Preliminaries

In a few-shot learning problem, we deal with tasks \mathcal{T}_i sampled from a task distribution $p(\mathcal{T})$. Each task \mathcal{T}_i is associated with a dataset \mathcal{D}_i , that we further subdivide into a support set $\mathcal{D}_i^s = (X_i^s, Y_i^s) = \{(\mathbf{x}_{i,r}^s, \mathbf{y}_{i,r}^s)\}_{r=1}^{N_s}$ and a query set $\mathcal{D}_i^q = (X_i^q, Y_i^q) = \{(\mathbf{x}_{i,r}^q, \mathbf{y}_{i,r}^q)\}_{r=1}^{N_q}$. Given a learning model f_θ , where θ denotes the model parameters, few-shot learning algorithms attempt to learn θ to minimize the loss on the query set \mathcal{D}_i^q for each of the sampled tasks using the data-label pairs from the corresponding support set \mathcal{D}_i^s . Thereafter, during the testing stage, the trained model f_θ and the support set \mathcal{D}_j^s for new tasks \mathcal{T}_j can be used to perform inference (and also evaluate the performance) on the corresponding query set \mathcal{D}_j^q . In the following subsections, we discuss two prominent few-shot learning strategies, namely gradient-based meta-learning and prototype-based metric-learning.

3.1 Gradient-based meta-learning

In gradient-based meta-learning, the aim is to learn initial parameters θ^* such that a typically small number of gradient update steps using the data-label pairs in the support set \mathcal{D}_i^s results in a model f_{ϕ_i} that performs well on the query set of task \mathcal{T}_i . During the meta-training stage, first a base learner is trained on multiple support sets \mathcal{D}_i^s , and the performance of the resulting models f_{ϕ_i} is evaluated on the corresponding query sets \mathcal{D}_i^q . The meta-learner parameters θ are then updated such that the expected loss of the base learner on query sets is minimized. In the meta-testing stage, the final meta-trained model f_{θ^*} is fine-tuned on the support set \mathcal{D}_j^s for the given test task \mathcal{T}_j to obtain the adapted model f_{ϕ_j} , that can then be used for inference on the corresponding query set

\mathcal{D}_i^q . Considering Model-Agnostic Meta-Learning (MAML) [5] as an example, the bi-level optimization of the gradient-based meta-learning can be formulated as:

$$\theta^* \leftarrow \arg \min_{\theta} \mathbb{E}_{\mathcal{T}_i \sim p(\mathcal{T})} [\mathcal{L}(f_{\phi_i}; \mathcal{D}_i^q)], \text{ where } \phi_i = \theta - \eta_0 \nabla_{\theta} \mathcal{L}(f_{\theta}; \mathcal{D}_i^s), \quad (1)$$

while η_0 denotes the inner-loop learning rate used by base learner to train on \mathcal{D}_i^s for task \mathcal{T}_i , and \mathcal{L} is the loss function, which is usually the cross-entropy loss for classification problems:

$$\mathcal{L}_{CE} = \mathbb{E}_{\mathcal{T}_i \sim p(\mathcal{T})} [-\sum_r \log p(\mathbf{y}_{i,r}^q | \mathbf{x}_{i,r}^q, f_{\phi_i})]. \quad (2)$$

3.2 Prototype-based metric-learning

The aim of metric-based few-shot learning is to obtain a feature embedding of the task manifold suitable for non-parametric classification. Prototype-based metric-learning, specifically Prototypical Network (ProtoNet) [22], uses a non-parametric classifier that assign a query point to the class having the nearest (in terms of Euclidean distance) prototype in the learned embedding space. Given the model f_{θ} and a task \mathcal{T}_i , we first compute class prototypes $\{\mathbf{c}_k\}_{k=1}^K$ as the mean of $f_{\theta}(\mathbf{x}_{i,r}^s)$ for the instances $\mathbf{x}_{i,r}^s$ belonging to class k :

$$\mathbf{c}_k = \frac{1}{N_s} \sum_{(\mathbf{x}_{i,r}^s, \mathbf{y}_{i,r}^s) \in \mathcal{D}_i^{s,k}} f_{\theta}(\mathbf{x}_{i,r}^s), \quad (3)$$

where $\mathcal{D}_i^{s,k} \subset \mathcal{D}_i^s$ represents the subset of N_s support samples from class k . Now given a sample $\mathbf{x}_{i,r}^q$ from the query set, the probability $p(\mathbf{y}_{i,r}^q = k | \mathbf{x}_{i,r}^q)$ of assigning it to the k -th class is calculated using the distance function $d(\cdot, \cdot)$ between the representation $f_{\theta}(\mathbf{x}_{i,r}^q)$ and the prototype \mathbf{c}_k for class k :

$$p(\mathbf{y}_{i,r}^q = k | \mathbf{x}_{i,r}^q, f_{\theta}) = \frac{\exp(-d(f_{\theta}(\mathbf{x}_{i,r}^q), \mathbf{c}_k))}{\sum_{k'} \exp(-d(f_{\theta}(\mathbf{x}_{i,r}^q), \mathbf{c}_{k'}))}. \quad (4)$$

Thereafter, the parameters θ for the model f_{θ} can be trained by minimizing cross-entropy loss (2). In the testing stage, each query sample $\mathbf{x}_{j,r}^q$ is assigned to the class having the maximal probability, i.e., $\mathbf{y}_{j,r}^q = \arg \max_k p(\mathbf{y}_{j,r}^q = k | \mathbf{x}_{j,r}^q)$.

A key requirement for effective few-shot generalization to new tasks for both gradient-based meta-learning and prototype-based metric-learning is to learn a good embedding of the high-dimensional manifold characterizing the task distribution $p(\mathcal{T})$, i.e. the task manifold. Ideally, the learned embedding should conserve the neighborhoods from the high-dimensional task manifold [24,20]. Hence, in the following subsection, we discuss Interval Bound Propagation (IBP) [6] that can be employed to define a neighborhood around a given task.

3.3 Interval bound propagation

Let us consider a neural network f_θ consisting of a sequence of transformations h_l , ($l \in \{1, 2, \dots, L\}$) for each of its L layers. We start from an initial input $\mathbf{z}_0 = \mathbf{x}$ to the network along with lower bound $\underline{\mathbf{z}}_0(\epsilon) = \mathbf{x} - \mathbf{1}\epsilon$ and upper bound $\bar{\mathbf{z}}_0(\epsilon) = \mathbf{x} + \mathbf{1}\epsilon$ for an ϵ -neighborhood around the input \mathbf{x} . In each of the subsequent layers $l \in \{1, 2, \dots, L\}$ of the network, we get an activation $\mathbf{z}_l = h_l(\mathbf{z}_{l-1})$. Additionally, IBP uses interval arithmetic to obtain the corresponding bounds on the activation \mathbf{z}_l for the l -th layer. The bounds are characterized by axis-aligned bounding boxes of the form $\underline{\mathbf{z}}_l(\epsilon) \leq \mathbf{z}_l \leq \bar{\mathbf{z}}_l(\epsilon)$ (where the relation \leq must hold individually for all coordinates of the vectors). Based on the specific nature of the transformation h_l in the l -th layer, interval arithmetic yields corresponding lower and upper bound transformations $\underline{\mathbf{z}}_l(\epsilon) = \underline{h}_l(\underline{\mathbf{z}}_{l-1}(\epsilon), \bar{\mathbf{z}}_{l-1}(\epsilon))$, and $\bar{\mathbf{z}}_l(\epsilon) = \bar{h}_l(\underline{\mathbf{z}}_{l-1}(\epsilon), \bar{\mathbf{z}}_{l-1}(\epsilon))$, such that each of the coordinates $\underline{z}_{l,c}(\epsilon)$ and $\bar{z}_{l,c}(\epsilon)$ of $\underline{\mathbf{z}}_l(\epsilon)$ and $\bar{\mathbf{z}}_l(\epsilon)$ respectively, satisfies the conditions:

$$\underline{z}_{l,c}(\epsilon) = \min_{\underline{\mathbf{z}}_{l-1}(\epsilon) \leq \mathbf{z}_{l-1} \leq \bar{\mathbf{z}}_{l-1}(\epsilon)} \mathbf{e}_c^T h_l(\mathbf{z}_{l-1}), \text{ and} \quad (5)$$

$$\bar{z}_{l,c}(\epsilon) = \max_{\underline{\mathbf{z}}_{l-1}(\epsilon) \leq \mathbf{z}_{l-1} \leq \bar{\mathbf{z}}_{l-1}(\epsilon)} \mathbf{e}_c^T h_l(\mathbf{z}_{l-1}), \quad (6)$$

where \mathbf{e}_c is the standard c -th basis vector. Further extending to multiple layers, such as the first S layers of the neural network f_{θ^S} , the individual transformations \underline{h}_l and \bar{h}_l for $l \in \{1, 2, \dots, S\}$ can be composed to respectively obtain the corresponding functions \underline{f}_{θ^S} and \bar{f}_{θ^S} , such that $\underline{\mathbf{z}}_S(\epsilon) = \underline{f}_{\theta^S}(\mathbf{z}_0, \epsilon)$, and $\bar{\mathbf{z}}_S(\epsilon) = \bar{f}_{\theta^S}(\mathbf{z}_0, \epsilon)$.

4 Proposed Method

The aim of the proposed method is to enable the learner f_θ to learn a feature embedding that attempts to preserve the ϵ -neighborhoods in the task manifold. Therefore, in the following subsections we describe the notion of an ϵ -neighborhood for a training task \mathcal{T}_i using IBP and show how they can be preserved to aid in few-shot learning problems.

4.1 Interval bounds for tasks

For a given training task \mathcal{T}_i , we define the ϵ -neighborhood of the task as consisting of the sets $\mathcal{I}_i^s(\epsilon)$ and $\mathcal{I}_i^q(\epsilon)$ of the interval bounds, respectively, of the data instances in the support set \mathcal{D}_i^s and the query set \mathcal{D}_i^q of the task, calculated at the S -th layer of the learner:

$$\mathcal{I}_i^s(\epsilon) = \{\underline{f}_{\theta^S}(\mathbf{x}_{i,r}^s, \epsilon)\}_{r=1}^{N_s} \cup \{\bar{f}_{\theta^S}(\mathbf{x}_{i,r}^s, \epsilon)\}_{r=1}^{N_s}, \text{ and} \quad (7)$$

$$\mathcal{I}_i^q(\epsilon) = \{\underline{f}_{\theta^S}(\mathbf{x}_{i,r}^q, \epsilon)\}_{r=1}^{N_q} \cup \{\bar{f}_{\theta^S}(\mathbf{x}_{i,r}^q, \epsilon)\}_{r=1}^{N_q}, \quad (8)$$

where $S (\leq L)$ is an user-specified layer number meant to demarcate the boundary between the portion f_{θ^S} of the model that focuses on feature representation and the subsequent portion $f_{\theta^{L-S}}$ responsible for the classification, such that $f_{\theta} = f_{\theta^{L-S}} \circ f_{\theta^S}$.

4.2 Few-shot learning with interval bounds

The Euclidean distances between the embedding $f_{\theta^S}(\mathbf{x}_{i,r}^q)$ for the query instances in a given training task \mathcal{T}_i and their respective interval bounds $\underline{f}_{\theta^S}(\mathbf{x}_{i,r}^q, \epsilon)$ and $\bar{f}_{\theta^S}(\mathbf{x}_{i,r}^q, \epsilon)$ is a measure of how well the ϵ -neighborhood of the task \mathcal{T}_i is preserved in the learned feature embedding:

$$\mathcal{L}_{LB} = \frac{1}{N_q} \sum_{r=1}^{N_q} \|f_{\theta^S}(\mathbf{x}_{i,r}^q) - \underline{f}_{\theta^S}(\mathbf{x}_{i,r}^q, \epsilon)\|_2^2 \text{ and} \quad (9)$$

$$\mathcal{L}_{UB} = \frac{1}{N_q} \sum_{r=1}^{N_q} \|f_{\theta^S}(\mathbf{x}_{i,r}^q) - \bar{f}_{\theta^S}(\mathbf{x}_{i,r}^q, \epsilon)\|_2^2. \quad (10)$$

In order to ensure that the small ϵ -neighborhoods get mapped to small interval bounds by the feature embedding f_{θ^S} , we can minimize the losses \mathcal{L}_{LB} and \mathcal{L}_{UB} in addition to the classification loss \mathcal{L}_{CE} in (2). It is important to notice that losses \mathcal{L}_{LB} and \mathcal{L}_{UB} are never used for the support instances $\mathbf{x}_{i,r}^s$.

Attempting to minimize a naïve sum of the three losses can cause some issues. For example, weighing the classification loss \mathcal{L}_{CE} too high essentially makes the proposed method boil-down to vanilla few-shot learning. On the other hand, weighing the interval losses \mathcal{L}_{LB} and/or \mathcal{L}_{UB} too high may diminish learnability as the preservation of ϵ -neighborhoods gets precedence over classification performance. Moreover, such static weighting approaches are not capable to adapt to (and consequently mitigate) situations where one of the losses comes to unduly dominate the others. Thus, we minimize a convex weighted sum \mathcal{L} of the three losses where the weight for each loss is dynamically calculated based on a softmax across the three loss values:

$$\mathcal{L}(t) = w_{CE}(t)\mathcal{L}_{CE}(t) + w_{LB}(t)\mathcal{L}_{LB}(t) + w_{UB}(t)\mathcal{L}_{UB}(t), \quad (11)$$

where t denotes the current training step and $w_e(t)$ is the weight for the corresponding loss \mathcal{L}_e , $e \in \{CE, LB, UB\}$ at the t -th training step calculated as:

$$w_e(t) = \frac{\exp(\mathcal{L}_e(t)/\gamma)}{\sum_{e' \in \{CE, LB, UB\}} \exp(\mathcal{L}_{e'}(t)/\gamma)}, \quad (12)$$

with the hyperparameter γ controlling the relative importance of the losses.

Recent works [28] have shown that task interpolation can be used to improve performance in domains with a limited amount of tasks. Therefore, in the following subsection, we further propose a novel method for creating artificial tasks based on the ϵ -neighborhoods obtained for each task using interval bounds.

4.3 Interval bound-based task interpolation

For few-shot learning problems with a limited number of available training tasks, artificial tasks can be created using interpolation and/or augmentation for more effective training [27,15,28]. Moreover, inter-task interpolation has been shown to be more effective than intra-task augmentation techniques [28]. However, for inter-task interpolation between two tasks, it is important to choose pairs of tasks which are close to each other, in order to restrict the artificial tasks to the vicinity of the task manifold (see Figure 2). Since minimizing the additional losses \mathcal{L}_{LB} and \mathcal{L}_{UB} is expected to ensure that the ϵ -neighborhood around a task is mapped to a small interval in the feature embedding space, artificial tasks formed within such intervals are naturally expected to be close to the task manifold. Therefore, we create additional artificial tasks by interpolating between an original task and its corresponding interval bounds (i.e., either the upper or the lower interval bound). In other words, for a training task \mathcal{T}_i , a corresponding artificial task \mathcal{T}'_i is characterized by a support set $\mathcal{D}_i^{s'} = \{(\mathbf{H}_{i,r}^{s'}, \mathbf{y}_{i,r}^s)\}_{r=1}^{N_s}$ in the embedding space. The artificial support instances $\mathbf{H}_{i,r}^{s'}$ are created as:

$$\mathbf{H}_{i,r}^{s'} = (1 - \lambda_k) f_{\theta^S}(\mathbf{x}_{i,r}^s) + (1 - \nu_k) \lambda_k \underline{f}_{\theta^S}(\mathbf{x}_{i,r}^s, \epsilon) + \nu_k \lambda_k \bar{f}_{\theta^S}(\mathbf{x}_{i,r}^s, \epsilon), \quad (13)$$

where k denotes the class to which $\mathbf{x}_{i,r}^s$ belongs, $\lambda_k \in [0, 1]$ is sampled from a Beta distribution $Beta(\alpha, \beta)$, and the random choice of $\nu_k \in \{0, 1\}$ dictates which of the bounds is chosen randomly for each class. The labels $\mathbf{y}_{i,r}^s$ for the artificial task remain identical to that of the original task. The query set $\mathcal{D}_i^{q'}$ for the artificial task is also constructed in an analogous manner. We then minimize the mean of the additional classification loss \mathcal{L}'_{CE} for the artificial task \mathcal{T}'_i and the classification loss \mathcal{L}_{CE} for the original task \mathcal{T}_i for query instances (also the support instances in case of meta-learning). As a reminder, the losses \mathcal{L}_{LB} and \mathcal{L}_{UB} are also additionally minimized for the query instances.

Putting it all together: The complete IBP and IBP-based task interpolation (IBPI) training setup is illustrated in Figure 3. The way in which the training support set \mathcal{D}_i^s informs the loss calculation on the corresponding query set \mathcal{D}_i^q differs between the MAML and ProtoNet variants. While a limited number of training steps on the support set is undertaken to obtain the model f_{ϕ_i} where the loss is calculated on the query set for MAML, the support set is used to calculate the prototypes $\{\mathbf{c}_k\}_{k=1}^K$ for the loss calculation on the query set for ProtoNet. The pseudocodes showing how the inclusion of IBP and IBPI alters the standard training setup for MAML and ProtoNet are presented in the supplementary document. Since neither simple IBP-aided learning nor IBPI plays any part during the testing phase, the testing recipes for both MAML and ProtoNet remain unaltered compared to their original versions [5,22].

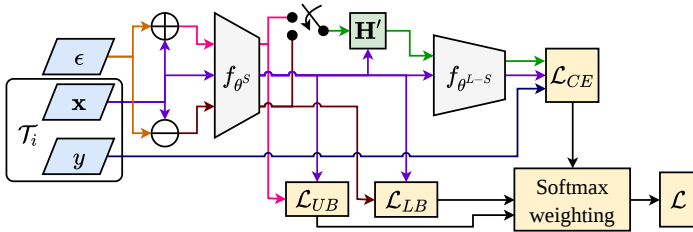


Fig. 3. Interval bound propagation-based few-shot training (best viewed in color): For each query data-label pair (\mathbf{x}, y) in a given training task \mathcal{T}_i , we start by defining a ϵ -neighborhood $[\mathbf{x} - \mathbf{1}\epsilon, \mathbf{x} + \mathbf{1}\epsilon]$ around \mathbf{x} . The bounding box $[\underline{f}_{\theta^S}(\mathbf{x}, \epsilon), \bar{f}_{\theta^S}(\mathbf{x}, \epsilon)]$ around the embedding $f_{\theta^S}(\mathbf{x})$ after the first S layers of the learner is found using IBP. In addition to the classification loss \mathcal{L}_{CE} , we also minimize the losses \mathcal{L}_{LB} and \mathcal{L}_{UB} which respectively measure the distances of $f_{\theta^S}(\mathbf{x})$ to $\underline{f}_{\theta^S}(\mathbf{x}, \epsilon)$ and $\bar{f}_{\theta^S}(\mathbf{x}, \epsilon)$. A softmax across the three loss values is used to dynamically calculate the convex weights for the losses, so as to prioritize the minimization of the dominant loss(es) at any given training step. Moreover, if IBP-based interpolation is used then artificial task \mathcal{T}'_i is created with instances \mathbf{H}' formed by interpolating both the support and query instances with their corresponding lower or upper bounds. In this case, the mean of the classification loss \mathcal{L}_{CE} for the \mathcal{T}_i and the corresponding extra loss \mathcal{L}'_{CE} for \mathcal{T}'_i is minimized.

5 Experiments

5.1 Experiment protocol

We empirically demonstrate the effectiveness of our proposed IBP and IBPI methods on the gradient-based meta-learning method MAML [5] and the prototype-based metric-learner ProtoNet [22]. We first investigate the scenario where the datasets have a large pool of available tasks using the few-shot classification benchmarks miniImageNet [26] and tieredImageNet [18]. Thereafter, to also analyse the impact of scarcity of tasks on the few-shot classification performance of IBP and IBPI, we conduct experiments on a subset of the miniImageNet dataset called miniImageNet-S [28], and two medical images datasets namely DermNet-S [28], and ISIC [4,11]. Finally, we also conduct a few analyses and ablations to better understand the properties of our proposed methods. For all our experiments, we employ the commonly used “4-CONV” [26] network containing 4 blocks of 64 convolutional kernels, batch normalization, max-pooling, and ReLU activation, followed by a final fully-connected layer. We perform 5-way 1-shot and 5-way 5-shot classification on all the above datasets (except ISIC where we use 2-way classification problems, similar to [27], due to the lack of sufficient training classes). Further discussion on the datasets, and implementation details of IBP and IBPI along with the choice of hyperparameters can be found in the supplementary document.

5.2 Results and discussion

Results on miniImageNet and tieredImageNet: As contending meta-learning algorithms, we choose the vanilla MAML along with notable meta-learners such as Meta-SGD [12], Reptile [16], LLAMA [7], R2-D2 [3], and BOIL [17]. Moreover, considering the regularizing effect of IBP and IBPI, we also include meta-learners such as TAML [8], Meta-Reg [29], and Meta-Dropout [10] which employ explicit regularization. We further include data augmentation-reliant learners such as MetaMix [27], Meta-Maxup [15], as well as the inter-task interpolation method MLTI [28]. In case of metric-learners, we compare against the vanilla ProtoNet in addition to other notable methods like MatchingNet [26], RelationNet [23], IMP [1], and GNN [21]. We also compare against ProtoNet coupled with data augmentation methods such as MetaMix, Meta-Maxup, and MLTI, as done in [28]. While [28] had to modify the training strategy of the canonical ProtoNet to accommodate the changes introduced by MetaMix, Meta-Maxup, and MLTI, the flexibility of IBP and IBPI imposes no such requirements. We summarize the findings in Table 1. We can observe that either IBP or IBPI or both achieve better Accuracy than the competitors in all cases. The slightly better performance of IBP with ProtoNet seems to imply that IBP-based task interpolation is often unnecessary for ProtoNet when a large number of tasks is available.

Results on few-task few-shot classification problems: For evaluating the few-shot classification performance of IBP and IBPI in few-task situations, we compare against the regularization based meta-learning methods TAML, Meta-Reg and Meta-Dropout for MAML. We also compare against data augmentation-based methods like MetaMix, Meta-Maxup, and MLTI for both MAML and ProtoNet. Overall, from Table 2 we observe that both IBP and IBPI outperform the other competitors, with the largest gains being observed for the ISIC dataset. For ProtoNet, we observe IBP and IBPI to be competitive with each other (as opposed to IBP being slightly better in many-task scenario), implying that there might be some additional advantage to be had from IBPI training on ProtoNet on datasets with few-tasks.

Importance of dynamic loss weighting: To validate the usefulness of softmax-based dynamic weighting of the three losses in IBP and IBPI, we first find the average weights for each loss in a dynamic weight run and then plug-in the respective values as static weights for new runs. All experiments in Table 3 are conducted on the miniImageNet dataset. From the upper half of Table 3, we can see that the three average weights are always distinct with a definite trend in that \mathcal{L}_{CE} gets maximum importance followed by \mathcal{L}_{UB} while \mathcal{L}_{LB} contributes very little to the total loss \mathcal{L} . This may be due to the particular “4-CONV” architecture that uses ReLU activations, thus implicitly limiting the spread of the lower bound [6]. Further, the average weights of IBP and IBPI are similar for a particular learner highlighting their commonalities, while they are distinct

Table 1. Performance comparison of the two proposed methods with baselines and competing algorithms on miniImageNet and tieredImageNet datasets. The results are reported in terms of mean Accuracy over 600 tasks with 95% confidence interval.

Dataset	Learner type	Algorithm	1-shot	5-shot
miniImageNet	Meta-learners	MAML [5]	48.70±1.75%	63.11±0.91%
		Meta-SGD [12]	50.47±1.87%	64.03±0.94%
		Reptile [16]	49.97±0.32%	65.99±0.58%
		LLAMA [7]	49.40±0.84%	-
		R2-D2 [3]	49.50±0.20%	65.40±0.20%
		TAML [8,28]	46.40±0.82%	63.26±0.68%
		BOIL [17]	49.61±0.16%	66.45±0.37%
		MAML+Meta-Reg [29,28]	47.02±0.77%	63.19±0.69%
		MAML+Meta-Dropout [10,28]	47.47±0.81%	64.11±0.71%
		MAML+MetaMix [27,28]	47.81±0.78%	64.22±0.68%
		MAML+Meta-Maxup [15,28]	47.68±0.79%	63.51±0.75%
		MAML+MLTI [28]	48.62±0.76%	64.65±0.70%
	Metric-learners	MAML+IBP (ours)	50.76±0.83%	67.13±0.81%
		MAML+IBPI (ours)	52.16±0.84%	67.56±0.86%
		MatchingNet [26]	43.44±0.77%	55.31±0.73%
		RelationNet [23]	50.44±0.82%	65.32±0.70%
		IMP [1]	49.60±0.80%	68.10±0.80%
		GNN [21]	49.02±0.98%	63.50±0.84%
		ProtoNet [22]	49.42±0.78%	68.20±0.66%
		ProtoNet*+MetaMix [27,28]	47.21±0.76%	64.38±0.67%
		ProtoNet*+Meta-Maxup [15,28]	47.33±0.79%	64.43±0.69%
		ProtoNet*+MLTI [28]	48.11±0.81%	65.22±0.70%
tieredImageNet	Meta-learners	ProtoNet+IBP (ours)	50.48±0.83%	68.33±0.79%
		ProtoNet+IBPI (ours)	51.79±0.81%	68.46±0.79%
		MAML [5]	51.67±1.81%	70.30±0.08%
		Meta-SGD [12]	48.97±0.21%	66.47±0.21%
	Metric-learners	Reptile [16]	49.97±0.32%	65.99±0.58%
		BOIL [17]	49.35±0.26%	69.37±0.12%
		MAML+IBP (ours)	54.36±0.80%	71.30±0.77%
		MAML+IBPI (ours)	54.16±0.79%	71.00±0.84%
	Metric-learners	MatchingNet [26]	54.02±0.79%	70.11±0.82%
		RelationNet [23]	54.48±0.93%	71.32±0.78%
		ProtoNet [22]	53.31±0.20%	72.69±0.74%
	Metric-learners	ProtoNet+IBP (ours)	53.83±0.81%	75.26±0.83%
		ProtoNet+IBPI (ours)	55.16±0.77%	74.96±0.82%

* ProtoNet implementation as per [28].

Table 2. Performance comparison of the two proposed methods with baselines and competing algorithms on miniImageNet-S, ISIC, and DermNet-S datasets containing fewer tasks. The results are reported in terms of mean Accuracy over 600 tasks (the 95% confidence interval is detailed in the supplementary document).

Learner type	Algorithm	miniImageNet-S		ISIC		DermNet-S	
		1-shot	5-shot	1-shot	5-shot	1-shot	5-shot
Meta-learners	MAML [5]	38.27%	52.14%	57.59%	65.24%	43.47%	60.56%
	MAML+Meta-Reg [29,28]	38.35%	51.74%	58.57%	68.45%	45.01%	60.92%
	TAML [8,28]	38.70%	52.75%	58.39%	66.09%	45.73%	61.14%
	MAML+Meta-Dropout [10,28]	38.32%	52.53%	58.40%	67.32%	44.30%	60.86%
	MAML+MetaMix [27,28]	39.43%	54.14%	60.34%	69.47%	46.81%	63.52%
	MAML+Meta-Maxup [15,28]	39.28%	53.02%	58.68%	69.16%	46.10%	62.64%
	MAML+MLTI [28]	41.58%	55.22%	61.79%	70.69%	48.03%	64.55%
	MAML+IBP (ours)	41.30%	54.36%	64.91%	78.75%	48.33%	63.33%
Metric-learners	MAML+IBPI (ours)	42.20%	55.23%	68.58%	79.75%	49.13%	65.43%
	ProtoNet* [22,28]	36.26%	50.72%	58.56%	66.25%	44.21%	60.33%
	ProtoNet [22]	40.70%	53.16%	65.58%	75.25%	46.86%	62.03%
	ProtoNet*+MetaMix [27,28]	39.67%	53.10%	60.58%	70.12%	47.71%	62.68%
	ProtoNet*+Meta-Maxup [15,28]	39.80%	53.35%	59.66%	68.97%	46.06%	62.97%
	ProtoNet*+MLTI [28]	41.36%	55.34%	62.82%	71.52%	49.38%	65.19%
	ProtoNet+IBP (ours)	41.46%	55.00%	70.75%	81.01%	48.66%	67.26%
	ProtoNet+IBPI (ours)	43.30%	55.73%	70.25%	81.16%	51.13%	65.93%

* ProtoNet implementation as per [28].

over different learners stressing their learner-dependent behavior. Further, in the lower half of Table 3, we explore the effect of using static weights as well as the transferability of the loss weights across learners. In all cases, the softmax-based dynamic weighting outperforms the static weighting, thus demonstrating the importance of the dynamic weighting. However, the static weighted ProtoNet+IBP variant performs better with the average weighting for MAML+IBP than that of its own, suggesting that the optimal static weighting may be different from the average of the dynamic weights for the corresponding run in some scenarios.

Table 3. Average loss weights for the two proposed methods, and a comparison of the static weighting and dynamic weighting versions, including the transferability of static weight values across variants (all experiments on miniImageNet).

Average of dynamic loss weights calculated for IBP and IBPI.				
	MAML+IBP	ProtoNet+IBP	MAML+IBPI	ProtoNet+IBPI
Weight for the classification loss, w_{CE}	0.9531	0.7715	0.9540	0.7714
Weight for the upper bound loss, w_{UB}	0.0469	0.1375	0.0459	0.1371
Weight for the lower bound loss, w_{LB}	42.4E-6	90.9E-3	32.4E-6	91.5E-3
Accuracy of algorithms with different weight choices.				
Weight choice	MAML+IBP	ProtoNet+IBP	MAML+IBPI	ProtoNet+IBPI
dynamic (from Table 1)	50.76%	51.79%	52.16%	50.48%
Static average weights for MAML+IBP	49.93%	49.23%	-	-
Static weights for ProtoNet+IBP	49.80%	48.73%	-	-
Static average weights for MAML+IBPI	-	-	50.20%	49.06%
Static average weights for ProtoNet+IBPI	-	-	49.10%	49.56%

Ablation on task interpolation: We undertake an ablation study to highlight the importance of generating artificial tasks using IBP bound-based interpolation by comparing IBPI with (1) inter-task interpolation on images, (2) inter-task interpolation in the feature embedding learned by f_{θ}^S , (3) MLTI [28], which performs MixUp [30] at randomly chosen layers of the learner, and (4) IBP bound-based interpolation without minimizing the \mathcal{L}_{UB} and \mathcal{L}_{LB} while only optimizing \mathcal{L}_{CE} . We perform the ablation study on miniImageNet and DermNet-S to compare the performance on different domains as well as to cover both the many-task and few-task scenarios. From Table 4, we observe that IBPI performs best in all cases. Moreover, inter-class interpolation at the same fixed layer S as IBPI and at randomly selected task-specific layers in MLTI shows worse performance, demonstrating the superiority of the proposed interval bound-based interpolation mechanism. Further, it is interesting to observe that IBPI, when performed without minimizing the \mathcal{L}_{UB} and \mathcal{L}_{LB} , performs the worst. This behavior is not unexpected as the neighborhoods are no longer guaranteed to be preserved by the learned embedding in this case, thus potentially resulting in the generation of out-of-manifold artificial tasks.

Study on compactness of the learned embedding: We gather the output of f_{θ^S} for 100 query instances in a 5-way 1-shot classification setting over 600 tasks

Table 4. Performance comparison of MAML+IBPI against inter-task interpolation on images, at a fixed intermediate layer S , MLTI [28], and interpolation with IBP bounds while only \mathcal{L}_{CE} (and not \mathcal{L}_{LB} and \mathcal{L}_{UB}) is minimized, in the 5-way 1-shot setting. The results are reported in terms of mean Accuracy over 600 tasks along with the 95% confidence intervals.

Algorithm	miniImageNet	DermNet-S
MAML+Inter-task interpolation on images	50.33 \pm 0.83%	48.30 \pm 0.81%
MAML+Inter-task interpolation after $f_{\theta S}$	50.83 \pm 0.82%	47.43 \pm 0.78%
MAML+MLTI [28]	48.62 \pm 0.76%	48.03 \pm 0.80%
MAML+IBPI without $\mathcal{L}_{LB}, \mathcal{L}_{UB}$ losses	48.20 \pm 0.77%	41.30 \pm 0.81%
MAML+IBPI (ours)	52.16\pm0.84%	49.13\pm0.80%

and calculate the average Euclidean distance with the nearest neighbor within the same class to observe the effects of IBP and IBPI training on the intra-task compactness in the feature embedding. In Table 5, we can observe that IBP and IBPI both result in more compact task representation in the learned feature space. The effect of IBP and IBPI are more prominent on datasets containing fewer tasks suggesting their ability to better regularize the learned feature embedding in such cases. Interestingly, IBP achieves better compactness than IBPI in almost all cases even though IBPI may have greater Accuracy as seen in Table 1-3. This suggests that an overtly compact feature embedding may be somewhat hard to classify. IBPI, on the other hand, seems to learn an embedding that is suitable for easier classification while still being relatively compact.

Table 5. Comparison of the Euclidean distance of the nearest neighbor from the same class for the feature embedding learned by $f_{\theta S}$. The table reports the mean and standard deviation of the nearest neighbor distances for 100 query instances in a 5-way 1-shot classification settings for 600 tasks as an indicator of intra-task compactness.

Algorithm	Dataset			
	miniImageNet	miniImageNet-S	tieredImageNet	DermNet-S
MAML	0.97 \pm 0.02	1.02 \pm 0.02	0.98 \pm 0.02	0.90 \pm 0.04
MAML-IBP (ours)	0.90 \pm 0.02	0.82 \pm 0.03	0.96 \pm 0.02	0.85 \pm 0.04
MAML-IBPI (ours)	0.94 \pm 0.02	0.86 \pm 0.03	0.95 \pm 0.02	0.89 \pm 0.04
ProtoNet	3.85 \pm 0.12	3.87 \pm 0.11	3.72 \pm 0.12	3.10 \pm 0.14
ProtoNet-IBP (ours)	3.84 \pm 0.11	3.41 \pm 0.10	3.66 \pm 0.11	2.68 \pm 0.10
ProtoNet-IBPI (ours)	3.84 \pm 0.12	3.59 \pm 0.11	3.70 \pm 0.12	2.58 \pm 0.10

Cross-domain transferability analysis: The miniImageNet-S, miniImageNet, tieredImageNet, and DermNet-S datasets all allow 5-way few-shot classification. Moreover, miniImageNet-S, miniImageNet and, tieredImageNet contain images from natural scenes while DermNet-S consists of medical images. Therefore, we undertake a cross-domain transferability study in Table 6. We summarize the Accuracy values obtained by a source model trained on DermNet-S and tested on miniImageNet-S, miniImageNet, and tieredImageNet and vice-versa. We can see that in all cases IBPI achieved the best performance, followed by IBP, showing

that IBP and IBPI training can both improve cross-domain transferability. Moreover, the performance on DermNet-S gradually improves for both the baselines and the proposed methods as the source model is trained on datasets offering an increasing number of tasks, implying the general requirement for a larger pool of tasks for ease of cross-domain transferability.

Table 6. Transferability comparison of MAML and ProtoNet, with their IBP and IBPI variants. All results are reported in terms of Accuracy over 600 tasks (the 95% confidence intervals are detailed in the supplementary document). For this table, DS, mIS, mI, and tI, will respectively mean DermNet-S, miniImageNet-S, miniImageNet, and tieredImageNet. Further, $A \rightarrow B$ indicates the model trained on dataset A is tested on dataset B .

Meta-learner	Accuracy			Metric-learner	Accuracy		
	DS \rightarrow mIS	DS \rightarrow mI	DS \rightarrow tI		DS \rightarrow mIS	DS \rightarrow mI	DS \rightarrow tI
MAML	25.06%	25.86%	26.90%	ProtoNet	28.76%	29.46%	29.43%
MAML+IBP (ours)	27.06%	27.13%	28.40%	ProtoNet+IBP (ours)	29.60%	29.73%	30.13%
MAML+IBPI (ours)	29.23%	29.23%	30.30%	ProtoNet+IBPI (ours)	30.33%	30.96%	31.50%
Meta-learner	mIS \rightarrow DS mI \rightarrow DS tI \rightarrow DS			Metric-learner	mIS \rightarrow DS mI \rightarrow DS tI \rightarrow DS		
	DS \rightarrow mIS	DS \rightarrow mI	DS \rightarrow tI		DS \rightarrow mIS	DS \rightarrow mI	DS \rightarrow tI
MAML	33.40%	34.26%	38.80%	ProtoNet	34.03%	37.46%	41.43%
MAML+IBP (ours)	33.90%	39.23%	39.73%	ProtoNet+IBP (ours)	34.03%	39.23%	42.83%
MAML+IBPI (ours)	34.76%	39.93%	40.50%	ProtoNet+IBPI (ours)	34.13%	40.00%	43.60%

6 Conclusion

In this paper, we attempt to explore the utility of IBP beyond its originally-intended usage for building and verifying classifiers that are provably robust against adversarial attacks. In summary, we identify the potential of IBP to conserve a neighborhood from the input image space to the learned feature space through the layers of a deep neural network by minimizing the distances of the feature embedding from the two bounds. We show how this can be effective in few-shot classification problems to obtain feature embeddings where task neighborhoods are preserved, thus enabling easy adaptability to unseen tasks. Further, since interpolating between training tasks and their corresponding IBP bounds can yield artificial tasks with a higher chance of lying on the task manifold, we exploit this property of IBP to prevent overfitting to seen tasks in the few-task scenario. The resulting IBP and IBPI training schemes are effective on both the meta-learning and metric-learning paradigms of few-shot learning.

Limitations and future work: One of the limitations of the proposed methods is that the computational cost of IBP scales linearly with the depth of the network. This has compelled us to restrict our investigation to the “4-CONV” backbone. Therefore, a future direction of research may be to investigate the applicability of more advanced provably robust training methods that yield more

efficient and tighter bounds than IBP while limiting the complexity and computational cost [13]. Moreover, few-shot learners can also be improved with adaptive hyperparameters [2], feature reconstruction [9], knowledge distillation [25], embedding propagation [19], etc. Thus, it may be interesting to observe the performance gains from these orthogonal techniques when coupled with IBP and IBPI. However, this may not be a straight-forward endeavor, given the complex dynamic nature of such frameworks.

References

1. Allen, K., Shelhamer, E., Shin, H., Tenenbaum, J.: Infinite mixture prototypes for few-shot learning. In: International Conference on Machine Learning. pp. 232–241. PMLR (2019)
2. Baik, S., Choi, M., Choi, J., Kim, H., Lee, K.M.: Meta-learning with adaptive hyperparameters. *Advances in Neural Information Processing Systems* **33**, 20755–20765 (2020)
3. Bertinetto, L., Henriques, J.F., Torr, P., Vedaldi, A.: Meta-learning with differentiable closed-form solvers. In: International Conference on Learning Representations (2019)
4. Codella, N.C., Gutman, D., Celebi, M.E., Helba, B., Marchetti, M.A., Dusza, S.W., Kalloo, A., Liopyris, K., Mishra, N., Kittler, H., et al.: Skin lesion analysis toward melanoma detection: A challenge at the 2017 international symposium on biomedical imaging (isbi), hosted by the international skin imaging collaboration (isic). In: 2018 IEEE 15th international symposium on biomedical imaging (ISBI 2018). pp. 168–172. IEEE (2018)
5. Finn, C., Abbeel, P., Levine, S.: Model-agnostic meta-learning for fast adaptation of deep networks. In: International conference on machine learning. pp. 1126–1135. PMLR (2017)
6. Goyal, S., Dvijotham, K.D., Stanforth, R., Bunel, R., Qin, C., Uesato, J., Arandjelovic, R., Mann, T., Kohli, P.: Scalable verified training for provably robust image classification. In: Proceedings of the IEEE/CVF International Conference on Computer Vision (ICCV) (October 2019)
7. Grant, E., Finn, C., Levine, S., Darrell, T., Griffiths, T.: Recasting gradient-based meta-learning as hierarchical bayes. In: International Conference on Learning Representations (2018)
8. Jamal, M.A., Qi, G.J.: Task agnostic meta-learning for few-shot learning. In: Proceedings of the IEEE/CVF Conference on Computer Vision and Pattern Recognition. pp. 11719–11727 (2019)
9. Lee, D.H., Chung, S.Y.: Unsupervised embedding adaptation via early-stage feature reconstruction for few-shot classification. In: International Conference on Machine Learning. pp. 6098–6108. PMLR (2021)
10. Lee, H.B., Nam, T., Yang, E., Hwang, S.J.: Meta dropout: Learning to perturb latent features for generalization. In: International Conference on Learning Representations (2020)
11. Li, X., Yu, L., Jin, Y., Fu, C.W., Xing, L., Heng, P.A.: Difficulty-aware meta-learning for rare disease diagnosis. In: International Conference on Medical Image Computing and Computer-Assisted Intervention. pp. 357–366. Springer (2020)
12. Li, Z., Zhou, F., Chen, F., Li, H.: Meta-SGD: Learning to learn quickly for few-shot learning. arXiv preprint arXiv:1707.09835 (2017)

13. Lyu, Z., Guo, M., Wu, T., Xu, G., Zhang, K., Lin, D.: Towards evaluating and training verifiably robust neural networks. In: Proceedings of the IEEE/CVF Conference on Computer Vision and Pattern Recognition (CVPR). pp. 4308–4317 (June 2021)
14. Van der Maaten, L., Hinton, G.: Visualizing data using t-sne. *Journal of machine learning research* **9**(11) (2008)
15. Ni, R., Goldblum, M., Sharaf, A., Kong, K., Goldstein, T.: Data augmentation for meta-learning. In: International Conference on Machine Learning. pp. 8152–8161. PMLR (2021)
16. Nichol, A., Achiam, J., Schulman, J.: On first-order meta-learning algorithms. arXiv preprint arXiv:1803.02999 (2018)
17. Oh, J., Yoo, H., Kim, C., Yun, S.Y.: {BOIL}: Towards representation change for few-shot learning. In: International Conference on Learning Representations (2021)
18. Ren, M., Triantafillou, E., Ravi, S., Snell, J., Swersky, K., Tenenbaum, J.B., Larochelle, H., Zemel, R.S.: Meta-learning for semi-supervised few-shot classification. arXiv preprint arXiv:1803.00676 (2018)
19. Rodríguez, P., Laradji, I., Drouin, A., Lacoste, A.: Embedding propagation: Smoother manifold for few-shot classification. In: European Conference on Computer Vision. pp. 121–138. Springer (2020)
20. Roweis, S.T., Saul, L.K.: Nonlinear dimensionality reduction by locally linear embedding. *Science* **290**(5500), 2323–2326 (2000)
21. Satorras, V.G., Estrach, J.B.: Few-shot learning with graph neural networks. In: International Conference on Learning Representations (2018)
22. Snell, J., Swersky, K., Zemel, R.: Prototypical networks for few-shot learning. *Advances in neural information processing systems* **30** (2017)
23. Sung, F., Yang, Y., Zhang, L., Xiang, T., Torr, P.H., Hospedales, T.M.: Learning to compare: Relation network for few-shot learning. In: Proceedings of the IEEE Conference on Computer Vision and Pattern Recognition (CVPR) (June 2018)
24. Tenenbaum, J.B., Silva, V.d., Langford, J.C.: A global geometric framework for nonlinear dimensionality reduction. *Science* **290**(5500), 2319–2323 (2000)
25. Tian, Y., Wang, Y., Krishnan, D., Tenenbaum, J.B., Isola, P.: Rethinking few-shot image classification: a good embedding is all you need? In: European Conference on Computer Vision. pp. 266–282. Springer (2020)
26. Vinyals, O., Blundell, C., Lillicrap, T., Wierstra, D., et al.: Matching networks for one shot learning. *Advances in neural information processing systems* **29** (2016)
27. Yao, H., Huang, L.K., Zhang, L., Wei, Y., Tian, L., Zou, J., Huang, J., et al.: Improving generalization in meta-learning via task augmentation. In: International Conference on Machine Learning. pp. 11887–11897. PMLR (2021)
28. Yao, H., Zhang, L., Finn, C.: Meta-learning with fewer tasks through task interpolation. In: International Conference on Learning Representations (2022)
29. Yin, M., Tucker, G., Zhou, M., Levine, S., Finn, C.: Meta-learning without memorization. arXiv preprint arXiv:1912.03820 (2019)
30. Zhang, H., Cisse, M., Dauphin, Y.N., Lopez-Paz, D.: mixup: Beyond empirical risk minimization. arXiv preprint arXiv:1710.09412 (2017)